A conservative lubrication dynamics method for the simulation of dense non-colloidal suspensions with particle spin

S. S. Prasanna Kumar[a,*], A. Vázquez-Quesada[b,c], M. Ellero[d,e,f]

[a]*Basque Center for Applied Mathematics (BCAM), Alameda de Mazarblacko 14, 48009 Bilbao, Spain*
[b]*Department of Theoretical Condensed Matter Physics, Universidad Autónoma de Madrid, Madrid, Spain*
[c]*Departamento de Física y Matemáticas, Universidad de Alcalá, 28871 Madrid, Spain*
[d]*Basque Center for Applied Mathematics (BCAM), Alameda de Mazarblacko 14, 48009 Bilbao, Spain*
[e]*IKERBASQUE, Basque Foundation for Science, Calle de María Díaz de Haro 3, 48013 Bilbao, Spain*
[f]*Zienkiewicz Centre for Computational Engineering (ZCCE), Swansea University, Bay Campus, Swansea SA1 8EN, United Kingdom*

Abstract

In this paper, a novel semi-implicit lubrication dynamics method that can efficiently simulate dense non-colloidal suspensions is proposed. To blackuce the computational cost in the presented methodology, inter-particle lubrication-based forces and torques alone are consideblack together with a short-range repulsion to enforce finite inter-particle separation due to surface roughness, Brownian forces or other excluded volume effects. Given that the lubrication forces are singular, i.e. scaling inversely with the inter-particle gap, the strategy to expedite the calculations is severely compromised if explicit integration schemes are used, especially at high concentrations. To overcome this issue, an efficient semi-implicit splitting integration scheme to solve for the particles translational and rotational velocities is presented. To validate the proposed methodology, a suspension under simple shear test is simulated in three dimensions and its rheology is compablack against benchmark results. To demonstrate the stability/speed-up in the calculations, performance of the proposed semi-implicit scheme is compablack against a classical explicit Velocity-Verlet scheme. The pblackicted viscometric functions for a non-colloidal suspension with a Newtonian matrix are in excellent agreement with the reference data from the literature. Moreover, the presented semi-implicit algorithm is found to be significantly faster than the classical lubrication dynamics methods with Velocity-Verlet integration schemes.

*Corresponding author
Email address: ssavarimuthu@bcamath.org (S. S. Prasanna Kumar)

Keywords:
numerical, rheology, non-colloidal, suspensions, complex fluids

1. Introduction

A wide variety of complex fluid-materials in the manufacturing and processing industries fall under the category of non-colloidal suspensions. Needless to say, developing an understanding of the behavior of such materials under different conditions can have tremendous implications in various fields of engineering and technology [1]. A comprehensive experimental characterization of their material behavior is not straightforward and usually involve costly equipments and time consuming procedures. In addition, it is difficult to obtain generic results due to the specific physicochemical interactions between the solvent and the dispersed medium. Therefore, to enable a better understanding of their complex physical nature, it is necessary to employ simpler model systems. A key advantage of such systems is the possibility to do *in silico* testing by developing mathematical expressions for the interaction between the suspension constituents which can be solved numerically [2, 3].

In general, depending on the way the suspending medium is taken into account, there are two types of approaches for the numerical simulation of non-colloidal suspensions. One approach is to model the hydrodynamic contributions implicitly, a classic example of which is the Stokesian Dynamics (SD) method [4]. In the SD and its variants, the suspended particles' velocities and forces are equated through a grand resistance matrix which, at each time step, is inverted to calculate the solid particles velocities. The positions of the particles are then computed by explicit integration of their velocities using a Runge-Kutta method. The computational cost associated with the matrix inversion operations limited the number of particles employable in the original SD method. Therefore, variants of SD were proposed to blackuce the computational complexity of the method by modifying the costly construction and inversion of the far-field mobility matrix. One such early approach was the Accelerated Stokesian Dynamics (ASD) [5] method which scales as $\mathcal{O}(N\ ln\ N)$, where N is the number of suspended particles in the system, against the original SD with $\mathcal{O}(N^3)$ scaling. Taking inspiration from the work of Ball and Melrose [6], some recent studies have further simplified the computations with modification to the construction of the resistance tensor. The mod-

ified resistance tensor typically contains an isotropic tensor with self-drag like terms added to another tensor obtained through pairwise summation of the short-range lubrication interactions. Since the major contribution to the resistance matrix comes from the lubrication forces, these variants are termed as Fast Lubrication Dynamics (FLD) [7, 8] methods. These modifications solely expedite the calculations, on the other hand SD-type methods may encounter some difficulties, as they rely on the analytical solution of Stokes flow, which is of different application in finite particle inertia, arbitrary particle shapes, compressibility effects, transient effects or complex solvent media. Another important aspect that requires attention is the conservation properties of these different numerical approaches, i.e. conservation of the linear and angular momentum. Although all methods follow from the conservation equations in their differential form, they often resort to careful modification/truncation in their numerical model that helps to reproduce the experimentally observed rheology. For example, in some studies the viscosity parameter in the isotropic tensor term is set based on fits to experimental relative viscosity measurements. Although these approaches are well-motivated and provide means to simulate complicated particle-laden flows, it is somewhat difficult to deduce the conservation properties of these methods.

Another approach, that can alleviate some of the aforementioned difficulties associated with the SD based methods, is to consider the hydrodynamic effects of the suspending media explicitly. This requires the solution of the Navier-Stokes equations through a Direct Numerical Simulation (DNS) [9, 10, 11, 12, 13] procedure. However, even for simple systems such as the non-colloidal hard spherical particles suspended in a Newtonian medium, DNS approaches can run into several numerical difficulties. The foremost issue is the requirement to resolve the thin interstitial fluid region between the solid particles which can become very narrow with increasing solid volume fraction and/or the bulk velocity of the suspension. To deploy DNS of the suspension in a brute force manner, significantly high computational effort and resources are requiblack to adapt the mesh for moving boundaries and for mesh refinement and coarsening, which does eventually limit the system size and the time scales of the simulation. This is true also for the methods based on Lagrangian description of the solvent such as the Smoothed Particle Hydrodynamics (SPH) [14, 15, 16, 17, 18, 19], if no proper treatment of the near-field hydrodynamic interaction is consideblack.

In particular, the necessity to refine the mesh in the inter-particle gaps is avoided in Ref. [17] by using an analytical expression for the short-range hydrodynamic forces known as the lubrication force corrections. Despite the simplicity of incorporating this change in a DNS-based approach, it should be noted that the singular nature of the lubrication force terms can place significant numerical constraints, such as a restrictive time step, due to particle pairs that are at near contact separations. This is particularly severe for explicit schemes where stability and accuracy are largely dictated by the time step size. In order to overcome this numerical issue, Bian and Ellero [20] proposed an efficient semi-implicit splitting integration scheme for the lubrication forces, coupled to an SPH model describing the far-field hydrodynamic interactions, which is significantly faster and stable even for dense suspensions of very high solid volume fraction.

In this paper, we propose a new 3D semi-implicit lubrication dynamics method based on the model proposed by Ball and Melrose [6] taking into account uniquely the short-range lubrication hydrodynamic interactions. For this reason, the computational requirement are strongly blackuced compablack to Refs. [17, 20]. Along with the model, an efficient splitting integration scheme is presented for the accelerated and stable simulation of non-colloidal hard spheres suspended in a Newtonian matrix. The integration scheme is used to compute both the particle's linear and angular velocities implicitly. Moreover, the discrete model is constructed to fully respect the linear and angular momentum conservation properties and can be easily extended for simulating non-Brownian suspensions with non-Newtonian matrices [21, 22, 23]. On the flip side, the lack of explicit interaction with the solvent and far-field hydrodynamic interaction limits the accurate description to dense systems. It must be pointed out that, in the proposed method, the suspension flow is established exclusively through pairwise short-ranged lubrication-based particle-particle and wall-particle interactions. The influence of the matrix flow on the particles, which requires addition of a self-drag term for each particle, is neglected for reason owing to loss of exact linear momentum conservation of a pair-wisely interacting particle system. As a result, the proposed method can accurately simulate only *dense suspensions* and, simulating single or few particles and dilute suspensions are beyond its range of applicability. To this end, Section 2 describes the lubrication dynamics methodology adopted in the present study. The derivation of the semi-implicit

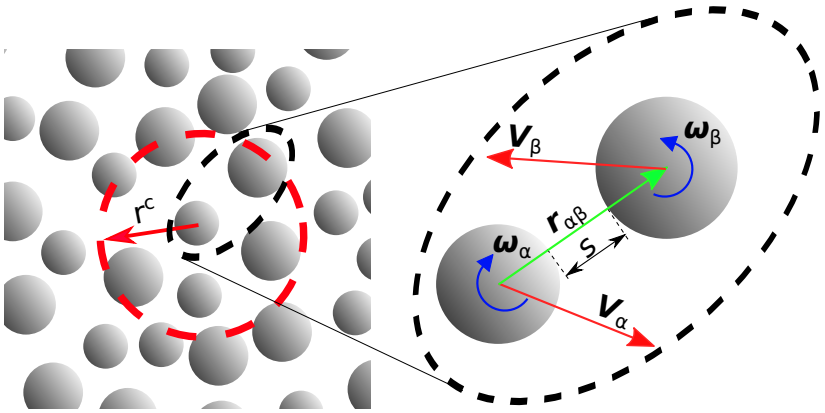

Figure 1: Schematic of a suspended particle-pair in a lubrication dynamics model.

integration scheme is briefly presented in Section 3. Using the presented methodology, simulation of the simple shear test was carried out and the results obtained are discussed in Section 4. The paper concludes with a brief summary highlighting the important findings of the present work in Section 5.

2. Modelling suspensions with lubrication dynamics

Numerical approaches like DNS and SD are excellent candidates for simulating suspensions, but, their requirement of computational resources and time increases prohibitively with particle volume fractions and system size. While it is imperative for the DNS approach to employ high performance computing to speed up the calculations, SD-type methods often resort to heuristic algorithmic simplifications. As these methods effectively and efficiently handle very low to moderate particle volume fractions and suffer high computational cost only at high volume fractions, there is an obvious necessity for alternative approaches tackling specifically higher particle concentrations. Taking advantage of the dominance of the lubrication forces over the long-range hydrodynamic interaction, we formulate a simple yet efficient approach to pblackict suspension rheology at high particle volume fractions. In this approach, we assume that only the squeezing and shearing flow in the narrow inter-particle gaps contribute towards the hydrodynamic effect on the particles. These can be implicitly accounted for through the short-range inter-particle lubrication forces, the expressions for which are readily available in the literature. Using these expressions, the contribution to the

total force on a given particle can be computed based on the interactions with its nearest neighbors which are determined through a cut-off distance r^c (see Fig. 1). In a similar manner, the total torque on a particle can also be calculated by summing the individual contribution from its nearest neighbors. Thereafter, for each particle in the suspension, the evolution of its translational and angular velocities are determined by integrating the summed inter-particle lubrication force and torque acting on it.

The most serious complication with this simplistic approach is due to the singular nature of the lubrication expressions. The leading order terms scale inversely with the inter-particle gap, denoted as s (see Fig. 1), which decreases with higher particle concentration and bulk velocity. This in turn results in diverging inter-particle lubrication forces and torques. Hence, special care has to be taken in choosing the appropriate time integration approach. It is possible to integrate naively using an explicit integration scheme, but the method would suffer from numerical instabilities, especially at higher particle concentrations, owing to severe restriction on the time step size. Therefore, an efficient integration approach is necessary to ensure the proposed method is faster while retaining its simplicity, accuracy and stability. Following the work of Bian and Ellero [20] a new fully conservative semi-implicit integration approach for particle systems with spin is developed in this study, the details of which are given in Section 3. Finally, the position vector of the particles can be simply obtained through explicit integration of its translational velocity.

It should also be pointed out that conservation of linear and angular momentum is of paramount importance for obtaining physically correct solutions. In the proposed lubrication-based model, we ensure that the conservation laws are obeyed by choosing the appropriate anti-symmetric expressions for the force and torque terms. The expressions used are presented and briefly discussed in the following section.

2.1. Lubrication force and torque

Various expressions for the lubrication force interaction has been employed in the literature. For a comprehensive review the reader is referblack to Ref. [24]. Taking into consideration the conservation of linear and angular momenta we have selected a specific set of expressions that satisfy geometrical conditions. For the present study, we follow the work of Ball and Melrose [6] and set the forces ($\boldsymbol{F}$) and torques ($\boldsymbol{T}$) on a given pair of spheres α

and β at very close separation as follows:

$$\boldsymbol{F}_\alpha = -\boldsymbol{F}_\beta = -a_{sq}\boldsymbol{e}_{\alpha\beta}\boldsymbol{e}_{\alpha\beta}\cdot\boldsymbol{v}_{\alpha\beta} - a_{sh}\left(\frac{2}{r_{\alpha\beta}}\right)^2(\mathbf{1}-\boldsymbol{e}_{\alpha\beta}\boldsymbol{e}_{\alpha\beta})\cdot\boldsymbol{v}_{\alpha\beta} - \frac{2}{r_{\alpha\beta}}a_{sh}\boldsymbol{e}_{\alpha\beta}\times(\boldsymbol{\omega}_\alpha+\boldsymbol{\omega}_\beta)\,, \quad (1)$$

$$\begin{aligned}\boldsymbol{T}_\alpha =& \frac{2}{r_{\alpha\beta}}a_{sh}\boldsymbol{e}_{\alpha\beta}\times(\mathbf{1}-\boldsymbol{e}_{\alpha\beta}\boldsymbol{e}_{\alpha\beta})\cdot\boldsymbol{v}_{\alpha\beta} - a_{sh}(\mathbf{1}-\boldsymbol{e}_{\alpha\beta}\boldsymbol{e}_{\alpha\beta})\cdot(\boldsymbol{\omega}_\alpha+\boldsymbol{\omega}_\beta) - \\ & a_{pu}(\mathbf{1}-\boldsymbol{e}_{\alpha\beta}\boldsymbol{e}_{\alpha\beta})\cdot\boldsymbol{\omega}_{\alpha\beta} - a_{tw}\boldsymbol{e}_{\alpha\beta}\boldsymbol{e}_{\alpha\beta}\cdot\boldsymbol{\omega}_{\alpha\beta} \quad (2)\end{aligned}$$

and

$$\begin{aligned}\boldsymbol{T}_\beta =& \frac{2}{r_{\alpha\beta}}a_{sh}\boldsymbol{e}_{\alpha\beta}\times(\mathbf{1}-\boldsymbol{e}_{\alpha\beta}\boldsymbol{e}_{\alpha\beta})\cdot\boldsymbol{v}_{\alpha\beta} - a_{sh}(\mathbf{1}-\boldsymbol{e}_{\alpha\beta}\boldsymbol{e}_{\alpha\beta})\cdot(\boldsymbol{\omega}_\alpha+\boldsymbol{\omega}_\beta) + \\ & a_{pu}(\mathbf{1}-\boldsymbol{e}_{\alpha\beta}\boldsymbol{e}_{\alpha\beta})\cdot\boldsymbol{\omega}_{\alpha\beta} + a_{tw}\boldsymbol{e}_{\alpha\beta}\boldsymbol{e}_{\alpha\beta}\cdot\boldsymbol{\omega}_{\alpha\beta}. \quad (3)\end{aligned}$$

Here, any quantity with subscript α or β represents the corresponding particle's quantity and any quantity with subscript $\alpha\beta$, say $A_{\alpha\beta}$ denotes $A_\alpha - A_\beta$. Therefore, $\boldsymbol{e}_{\alpha\beta}$ is the unit radial vector connecting a particle-pair, $r_{\alpha\beta}$ is the center-to-center particle distance, $\boldsymbol{v}_{\alpha\beta}$ is the relative velocity vector and $\boldsymbol{\omega}$ represents the angular velocity of the particles. For the case of spheres with equal radius a and inter-particle gap $s = r_{\alpha\beta} - 2a$, the co-efficients in the Eqs.(1), (2) and (3) are given in the following.

$$\begin{aligned}a_{sq} &= 3\pi\eta a\left(\frac{a}{2s}+\frac{18}{40}\ln\left(\frac{a}{s}\right)+\frac{9}{168}\frac{s}{a}\ln\left(\frac{a}{s}\right)\right)\\ a_{sh} &= \pi\eta a\frac{(2a+s)^2}{4}\ln\left(\frac{a}{s}\right)\\ a_{pu} &= \pi\eta a^3\left(\frac{3}{20}\ln\left(\frac{a}{s}\right)+\frac{63}{500}\frac{s}{a}\ln\left(\frac{a}{s}\right)\right)\\ a_{tw} &= \pi\eta a^3\left(\frac{s}{a}\ln\left(\frac{a}{s}\right)\right) \quad (4)\end{aligned}$$

Given that the inter-particle force is pairwise and antisymmetric i.e. $\boldsymbol{F}_\alpha = -\boldsymbol{F}_\beta$, the linear momentum of the particle system is directly conserved. In order to have angular momentum conservation, the condition $\boldsymbol{r}_{\alpha\beta}\times\boldsymbol{F}_\alpha + \boldsymbol{T}_\alpha + \boldsymbol{T}_\beta = 0$ should be satisfied. After some algebraic manipulations, it can be shown that the expressions given in Eqs. (1), (2) and (3) hold such a condition. Note that, unlike FLD-based approaches [7, 8], no particle self-drag term is consideblack in this formulation. Firstly, this avoids delicate tuning of the parameters, in fact the self-terms in FLD are selected to match the mean particle mobility (equivalently

the short time self-diffusivity) [25] and typically contains a macroscopic information on the whole suspension, i.e. $\eta(\phi)$ [26] which is one of the output properties of interest. Secondly, it also avoids the problem of lack of exact linear momentum conservation. To conserve linear momentum in a pair-wisely interacting particle system, the condition $\sum_i \sum_j F_{ij} = 0$ where index i goes over all the particles and j goes over the neighbors of i^{th} particle, needs to be satisfied. Adding a self-drag term systematically violates the aforementioned condition which in a pair-wisely interacting particle system with antisymmetric forces is automatically guaranteed.

2.2. Repulsive force

The flow of an ideal non-colloidal suspension is known to be a singular problem i.e. given that two particles are approaching each other, the inter-particle separation decreases indefinitely with no possible steady state. Consequently, the analytical solution for the problem pblackicts an increasingly large inter-particle dissipative force due to the squeezing of the interstitial fluid. However, in the case of real suspensions a finite inter-particle distance is reached owing to factors such as surface roughness, Brownian forces and other excluded volume effects. In the numerical simulations, these effects are accounted for through a short-range inter-particle repulsion force that helps to prevent unphysical particle overlapping. In the present study, a Derjaguin-Landau-Verwey-Overbeek [27, 28, 29] type repulsion for hard spheres is employed as given in the following.

$$\boldsymbol{F}^{rep}_{\alpha\beta} = F_0 \frac{\tau e^{-\tau h}}{1 - e^{-\tau h}} \boldsymbol{e}_{\alpha\beta} \tag{5}$$

Here, $h = \frac{s}{a}$ is the non-dimensional spacing between a particle-pair, F_0 is the peak magnitude of the repulsion force and τ determines its range. The value of $\tau = 10^3$ is typically chosen to model hard spheres, whereas $\tau = 10^2$ is used for soft repulsive interactions [28]. The suspension rheology, particularly at high particle volume fraction, is known to be significantly influenced by the repulsion force parameters and therefore needs to be heuristically set to match the experimental observations. Since the repulsion force depends only on the relative position of the particles a Verlet scheme is used for its integration.

3. Semi-implicit integration scheme

As mentioned earlier, the integration of the Eqs.(1), (2) and (3) for simulating dense suspensions of high particle concentration can become a computationally expensive task when explicit integration schemes are used. At high particle concentration, the near contact separation between the particles severely restricts the time step size leading to prolonged simulation duration. To resolve this issue, we present an efficient and robust semi-implicit integration scheme that can significantly speedup the simulation.

Consider the interaction between two spherical particles α and β of radius a, mass m and a moment of inertia I. At any given time t, if their translational velocities are $\boldsymbol{V}_\alpha$ and $\boldsymbol{V}_\beta$, and their angular velocities are $\boldsymbol{\omega}_\alpha$ and $\boldsymbol{\omega}_\beta$, their linear and angular velocities $\tilde{\boldsymbol{V}}_\alpha$, $\tilde{\boldsymbol{V}}_\beta$, $\tilde{\boldsymbol{\omega}}_\alpha$ and $\tilde{\boldsymbol{\omega}}_\beta$ after a time step Δt read

$$\tilde{\boldsymbol{V}}_\alpha = \boldsymbol{V}_\alpha + \tilde{\boldsymbol{F}}_\alpha \frac{\Delta t}{m} \tag{6}$$

$$\tilde{\boldsymbol{V}}_\beta = \boldsymbol{V}_\beta - \tilde{\boldsymbol{F}}_\alpha \frac{\Delta t}{m} \tag{7}$$

$$\tilde{\boldsymbol{\omega}}_\alpha = \boldsymbol{\omega}_\alpha + \tilde{\boldsymbol{T}}_\alpha \frac{\Delta t}{I} \tag{8}$$

$$\tilde{\boldsymbol{\omega}}_\beta = \boldsymbol{\omega}_\beta + \tilde{\boldsymbol{T}}_\beta \frac{\Delta t}{I}. \tag{9}$$

By subtracting the velocities and substituting (1) we find,

$$\tilde{\boldsymbol{V}}_{\alpha\beta} \cdot (A_{\alpha\beta} \boldsymbol{e}_{\alpha\beta} \boldsymbol{e}_{\alpha\beta} + B_{\alpha\beta} \boldsymbol{1}) + C_{\alpha\beta} \boldsymbol{e}_{\alpha\beta} \times (\tilde{\boldsymbol{\omega}}_\alpha + \tilde{\boldsymbol{\omega}}_\beta) = \boldsymbol{V}_{\alpha\beta} \tag{10}$$

where,

$$\begin{aligned} A_{\alpha\beta} &= 2\frac{\Delta t}{m}\left(a_{sq} - a_{sh}\left(\frac{2}{r_{\alpha\beta}}\right)^2\right) \\ B_{\alpha\beta} &= 1 + 2\frac{\Delta t}{m} a_{sh}\left(\frac{2}{r_{\alpha\beta}}\right)^2 \\ C_{\alpha\beta} &= \frac{2\Delta t}{m}\frac{2}{r_{\alpha\beta}} a_{sh} \end{aligned} \tag{11}$$

Similarly, by adding the angular velocities and substituting Eqs. (2) and (3) one obtains

$$D_{\alpha\beta} \boldsymbol{e}_{\alpha\beta} \times \tilde{\boldsymbol{V}}_{\alpha\beta} + (E_{\alpha\beta} \boldsymbol{1} + F_{\alpha\beta} \boldsymbol{e}_{\alpha\beta} \boldsymbol{e}_{\alpha\beta}) \cdot (\tilde{\boldsymbol{\omega}}_\alpha + \tilde{\boldsymbol{\omega}}_\beta) = \boldsymbol{\omega}_\alpha + \boldsymbol{\omega}_\beta \tag{12}$$

where,

$$D_{\alpha\beta} = -\frac{4}{r_{\alpha\beta}} a_{sh} \frac{\Delta t}{I} \tag{13}$$

$$E_{\alpha\beta} = 1 + 2a_{sh} \frac{\Delta t}{I} \tag{14}$$

$$F_{\alpha\beta} = -2a_{sh} \frac{\Delta t}{I}. \tag{15}$$

Taking the cross product of $\boldsymbol{e}_{\alpha\beta}$ and Eq. (12), and rearranging the terms, one obtains

$$\boldsymbol{e}_{\alpha\beta} \times (\tilde{\boldsymbol{\omega}}_\alpha + \tilde{\boldsymbol{\omega}}_\beta) = \frac{1}{E_{\alpha\beta}} \boldsymbol{e}_{\alpha\beta} \times (\boldsymbol{\omega}_\alpha + \boldsymbol{\omega}_\beta) - \frac{D_{\alpha\beta}}{E_{\alpha\beta}} (\boldsymbol{e}_{\alpha\beta}\boldsymbol{e}_{\alpha\beta} - \mathbf{1}) \cdot \tilde{\boldsymbol{V}}_{\alpha\beta} \tag{16}$$

which after substituting in (10) gives,

$$\tilde{\boldsymbol{V}}_{\alpha\beta} \cdot \left(\left(A_{\alpha\beta} - \frac{C_{\alpha\beta} D_{\alpha\beta}}{E_{\alpha\beta}} \right) \boldsymbol{e}_{\alpha\beta}\boldsymbol{e}_{\alpha\beta} + \left(B_{\alpha\beta} + \frac{C_{\alpha\beta} D_{\alpha\beta}}{E_{\alpha\beta}} \right) \mathbf{1} \right) = \boldsymbol{V}_{\alpha\beta} - \frac{C_{\alpha\beta}}{E_{\alpha\beta}} \boldsymbol{e}_{\alpha\beta} \times (\boldsymbol{\omega}_\alpha + \boldsymbol{\omega}_\beta)$$

The last equation is a linear system on $\tilde{\boldsymbol{V}}_{\alpha\beta}$ for which the solution can be obtained by inverting the matrix of the system

$$\left(A_{\alpha\beta} - \frac{C_{\alpha\beta} D_{\alpha\beta}}{E_{\alpha\beta}} \right) \boldsymbol{e}_{\alpha\beta}\boldsymbol{e}_{\alpha\beta} + \left(B_{\alpha\beta} + \frac{C_{\alpha\beta} D_{\alpha\beta}}{E_{\alpha\beta}} \right) \mathbf{1}. \tag{17}$$

Considering the inverse matrix is of the form $Y_{\alpha\beta}\mathbf{1} + Z_{\alpha\beta}\boldsymbol{e}_{\alpha\beta}\boldsymbol{e}_{\alpha\beta}$, where $Y_{\alpha\beta}$ and $Z_{\alpha\beta}$ are functions to be determined, we can find that

$$\begin{aligned} Y_{\alpha\beta} &= \frac{E_{\alpha\beta}}{C_{\alpha\beta} D_{\alpha\beta} + B_{\alpha\beta} E_{\alpha\beta}} \\ Z_{\alpha\beta} &= \frac{C_{\alpha\beta} D_{\alpha\beta} - A_{\alpha\beta} E_{\alpha\beta}}{(A_{\alpha\beta} + B_{\alpha\beta})(C_{\alpha\beta} D_{\alpha\beta} + B_{\alpha\beta} E_{\alpha\beta})} \end{aligned} \tag{18}$$

Thus the relative velocity of a particle-pair after a given time step can be computed as follows.

$$\tilde{\boldsymbol{V}}_{\alpha\beta} = (Y_{\alpha\beta}\mathbf{1} + Z_{\alpha\beta}\boldsymbol{e}_{\alpha\beta}\boldsymbol{e}_{\alpha\beta}) \cdot \left(\boldsymbol{V}_{\alpha\beta} - \frac{C_{\alpha\beta}}{E_{\alpha\beta}} \boldsymbol{e}_{\alpha\beta} \times (\boldsymbol{\omega}_\alpha + \boldsymbol{\omega}_\beta) \right) \tag{19}$$

Using the conservation of the linear momentum i.e. $\tilde{\boldsymbol{V}}_\alpha + \tilde{\boldsymbol{V}}_\beta = \boldsymbol{V}_\alpha + \boldsymbol{V}_\beta$, the particles' individual velocities can be calculated as

$$\tilde{\boldsymbol{V}}_\beta = \frac{1}{2} \left(\boldsymbol{V}_\alpha + \boldsymbol{V}_\beta - \tilde{\boldsymbol{V}}_{\alpha\beta} \right) \text{ and } \tilde{\boldsymbol{V}}_\alpha = \tilde{\boldsymbol{V}}_{\alpha\beta} + \boldsymbol{V}_\beta. \tag{20}$$

To calculate the angular velocities, we begin by rewriting (12) as in the following.

$$(E_{\alpha\beta}\mathbf{1} + F_{\alpha\beta}\boldsymbol{e}_{\alpha\beta}\boldsymbol{e}_{\alpha\beta}) \cdot (\tilde{\boldsymbol{\omega}}_\alpha + \tilde{\boldsymbol{\omega}}_\beta) = \boldsymbol{\omega}_\alpha + \boldsymbol{\omega}_\beta - D_{\alpha\beta} Y_{\alpha\beta} \left(\boldsymbol{e}_{\alpha\beta} \times \boldsymbol{V}_{\alpha\beta} - \frac{C_{\alpha\beta}}{E_{\alpha\beta}} (\boldsymbol{e}_{\alpha\beta}\boldsymbol{e}_{\alpha\beta} - \mathbf{1}) \cdot (\boldsymbol{\omega}_\alpha + \boldsymbol{\omega}_\beta) \right) \tag{21}$$

Using the the inverse of the matrix $(E_{\alpha\beta}\mathbf{1} + F_{\alpha\beta}\boldsymbol{e}_{\alpha\beta}\boldsymbol{e}_{\alpha\beta})$ given by

$$\frac{1}{E_{\alpha\beta}}\left[\mathbf{1} - \frac{F_{\alpha\beta}}{(E_{\alpha\beta}+F_{\alpha\beta})}\boldsymbol{e}_{\alpha\beta}\boldsymbol{e}_{\alpha\beta}\right] \tag{22}$$

in Eq. (21), we find

$$\tilde{\boldsymbol{\omega}}_\alpha + \tilde{\boldsymbol{\omega}}_\beta = [M_{\alpha\beta}\mathbf{1} + N_{\alpha\beta}\boldsymbol{e}_{\alpha\beta}\boldsymbol{e}_{\alpha\beta}]\cdot(\boldsymbol{\omega}_\alpha + \boldsymbol{\omega}_\beta) - P_{\alpha\beta}\boldsymbol{e}_{\alpha\beta}\times\boldsymbol{V}_{\alpha\beta} \tag{23}$$

where,

$$\begin{aligned} M_{\alpha\beta} &= \frac{1}{E_{\alpha\beta}}\left(1 - \frac{D_{\alpha\beta}Y_{\alpha\beta}C_{\alpha\beta}}{E_{\alpha\beta}}\right) \\ N_{\alpha\beta} &= \frac{1}{E_{\alpha\beta}}\left(\frac{D_{\alpha\beta}Y_{\alpha\beta}C_{\alpha\beta}}{E_{\alpha\beta}} - \frac{F_{\alpha\beta}}{E_{\alpha\beta}+F_{\alpha\beta}}\right) \\ P_{\alpha\beta} &= \frac{D_{\alpha\beta}Y_{\alpha\beta}}{E_{\alpha\beta}+F_{\alpha\beta}} \end{aligned} \tag{24}$$

Using $\boldsymbol{T}_{\alpha\beta}$ calculated from Eqs. (2) and (3), we determine from (8) and (9) that

$$\tilde{\boldsymbol{\omega}}_{\alpha\beta}\cdot[G_{\alpha\beta}\mathbf{1} + H_{\alpha\beta}\boldsymbol{e}_{\alpha\beta}\boldsymbol{e}_{\alpha\beta}] = \boldsymbol{\omega}_{\alpha\beta} \tag{25}$$

where

$$\begin{aligned} G_{\alpha\beta} &= \left(1 + 2a_{pu}\frac{\Delta t}{I}\right) \text{ and} \\ H_{\alpha\beta} &= 2\left(a_{tw} - a_{pu}\right)\frac{\Delta t}{I}. \end{aligned} \tag{26}$$

The inverse matrix of $G_{\alpha\beta}\mathbf{1} + H_{\alpha\beta}\boldsymbol{e}_{\alpha\beta}\boldsymbol{e}_{\alpha\beta}$ reads

$$\frac{1}{G_{\alpha\beta}}\left(\mathbf{1} - \frac{H_{\alpha\beta}}{G_{\alpha\beta}+H_{\alpha\beta}}\boldsymbol{e}_{\alpha\beta}\boldsymbol{e}_{\alpha\beta}\right) \tag{27}$$

and therefore we get,

$$\tilde{\boldsymbol{\omega}}_{\alpha\beta} = \frac{1}{G_{\alpha\beta}}\left(\mathbf{1} - \frac{H_{\alpha\beta}}{G_{\alpha\beta}+H_{\alpha\beta}}\boldsymbol{e}_{\alpha\beta}\boldsymbol{e}_{\alpha\beta}\right)\cdot\boldsymbol{\omega}_{\alpha\beta} \tag{28}$$

Finally, solving Eqs. (23) and (28), the individual angular velocity of the particles are found to be

$$\begin{aligned} \tilde{\boldsymbol{\omega}}_\alpha &= \frac{1}{2}\left\{\frac{1}{G_{\alpha\beta}}\left(\mathbf{1} - \frac{H_{\alpha\beta}}{G_{\alpha\beta}+H_{\alpha\beta}}\boldsymbol{e}_{\alpha\beta}\boldsymbol{e}_{\alpha\beta}\right)\cdot\boldsymbol{\omega}_{\alpha\beta} + \right. \\ &\quad \left.[M_{\alpha\beta}\mathbf{1} + N_{\alpha\beta}\boldsymbol{e}_{\alpha\beta}\boldsymbol{e}_{\alpha\beta}]\cdot(\boldsymbol{\omega}_\alpha + \boldsymbol{\omega}_\beta) - P_{\alpha\beta}\boldsymbol{e}_{\alpha\beta}\times\boldsymbol{V}_{\alpha\beta}\right\} \\ \tilde{\boldsymbol{\omega}}_\beta &= \frac{1}{2}\left\{-\frac{1}{G_{\alpha\beta}}\left(\mathbf{1} - \frac{H_{\alpha\beta}}{G_{\alpha\beta}+H_{\alpha\beta}}\boldsymbol{e}_{\alpha\beta}\boldsymbol{e}_{\alpha\beta}\right)\cdot\boldsymbol{\omega}_{\alpha\beta} + \right. \\ &\quad \left.[M_{\alpha\beta}\mathbf{1} + N_{\alpha\beta}\boldsymbol{e}_{\alpha\beta}\boldsymbol{e}_{\alpha\beta}]\cdot(\boldsymbol{\omega}_\alpha + \boldsymbol{\omega}_\beta) - P_{\alpha\beta}\boldsymbol{e}_{\alpha\beta}\times\boldsymbol{V}_{\alpha\beta}\right\} \end{aligned} \tag{29}$$

The whole solution is obtained by iteratively solving Eqs. (19)-(20) and Eq. (29) for each interacting pair (α, β).

To maintain the accuracy of the method and its robustness at all particle configurations, the Δt in Eqs. (20) and (29) is replaced by $\Delta t_{sweep} = \Delta t / N_{sweep}$ in the implementation. Here, the number of sub-iteration N_{sweep} is dynamically determined to ensure it is high enough to get convergence while simultaneously being sufficiently small to speed up the calculations. Beginning with a large default value for N_{sweep}, at each time step say n^{th}, two different sweeps are carried-out with $N_{sweep} = 2^m$ and $N_{sweep} = 2^{m-1}$. Then, the difference in the particles' linear and angular velocities are computed through an L_2 norm defined as,

$$e_v^m = \frac{\sqrt{\sum_{\alpha=1}^{N} (\tilde{V}_\alpha^m - \tilde{V}_\alpha^{m-1})^2}}{\sqrt{\sum_{\alpha=1}^{N} (\tilde{V}_\alpha^m)^2}} \text{ and } e_\omega^m = \frac{\sqrt{\sum_{\alpha=1}^{N} (\tilde{\omega}_\alpha^m - \tilde{\omega}_\alpha^{m-1})^2}}{\sqrt{\sum_{\alpha=1}^{N} (\tilde{\omega}_\alpha^m)^2}} \tag{30}$$

and compablack against the value of a pblackefined tolerance ϵ. If the value of e_v^m and e_ω^m are less than the specified tolerance then the value of N_{sweep} is halved. This procedure is repeated for q times until $(e^{m-q}, e_\omega^{m-q}) > \epsilon$. Upon reaching this condition, the value of $N_{sweep} = 2^{m-q-1}$ becomes the default number of sweeps for the iteration of the next time step and the velocities obtained with $N_{sweep} = 2^{m-q-1}$ are retained. On the contrary, if the value of e_v^m and e_ω^m are greater than the specified tolerance then the value of N_{sweep} is doubled and the procedure is repeated for q times until $(e_v^{m+q}, e_\omega^{m+q}) < \epsilon$. Finally, the value of $N_{sweep} = 2^{m+q}$ is set the default value for the subsequent time steps and the velocities obtained with this value of N_{sweep} is retained. From the computed velocities, the particles' positions are then updated using any desiblack explicit integration approach A flow chart illustrates the proposed semi-implicit splitting integration procedure in Fig. 2. As a final remark, the reader can refer to Appendix B where the method is discussed within an SD modeling framework.

3.1. Analysis of the algorithmic complexity

To illustrate the efficiency of the proposed semi-implicit integration algorithm for the lubrication force and torque, against an explicit integration, the algorithmic complexity of the scheme is analyzed in this section. By counting the number of floating point operations, with $+, -, \times, \div$ as one count, $log()$ as two counts and $()^{power}$ as three counts, requiblack for

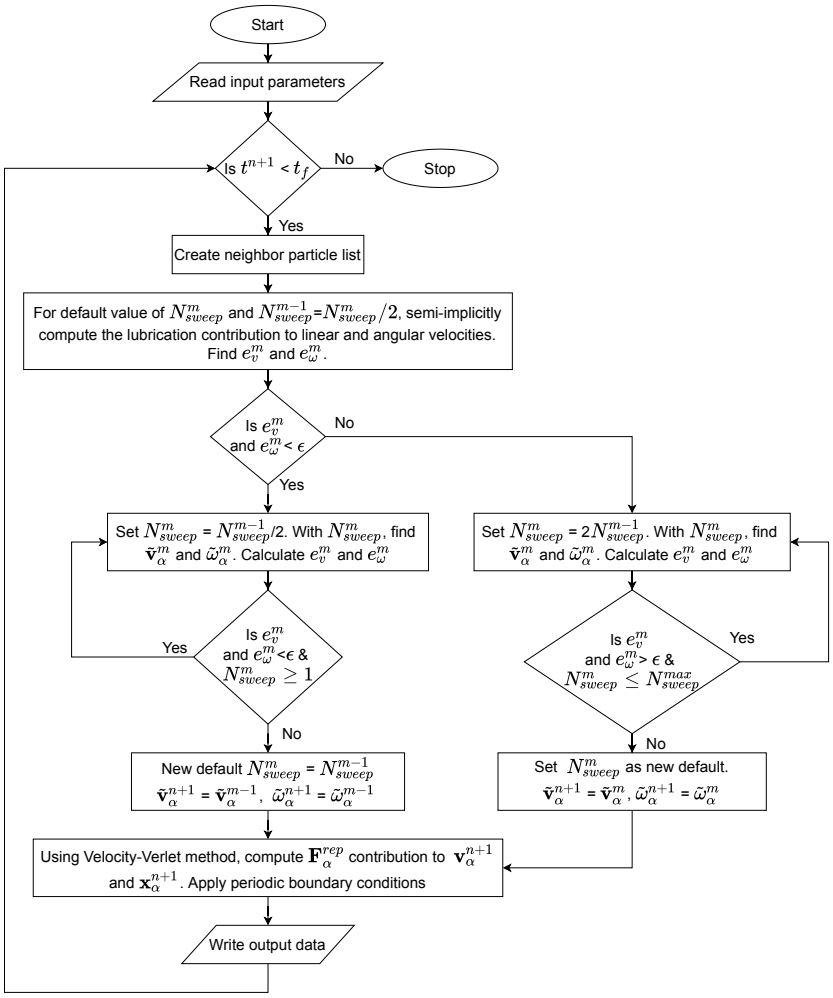

Figure 2: Flow chart of the proposed pairwise semi-implicit splitting integration procedure.

the computing the translational and angular velocities (see Table 1) a comparison is made between an explicit and the proposed semi-implicit integration algorithm. For the purpose of analysis, the Euler method is consideblack. The Euler method is the simplest of all integration scheme for explicit calculation of the particle velocities and therefore makes it easier to analyze the computational complexity involved. It also allows one to establish the most conservative algorithmic complexity expected from an explicit scheme to compare against the proposed method. However, it is pointed that a more accurate and more complex Velocity-Verlet method was used for obtaining the simulation results presented in the following sections. In other words, for the analysis, we compare with the least complex scheme (Euler), and in the simulations we compare with the more efficient scheme (Velocity-Verlet). Also, notice that

only the calculations that are distinct for each approach are consideblack for the analysis.

The algorithm begins with the neighbor search as shown in lines 1,2 and 3 of Table 1. Given that both the explicit and semi-implicit approach employ pairwise force and torque, the simplest direct neighbor search procedure would yield $N(N-1/2)$ possible pairs. From these pairs, finding the nearest neighbors based on the value of r^c would require 6 operations. The total number of operations involved in the rest of the calculations within the IF loop beginning in line 3 depend on the actual number of nearest neighbors (N_{neigh}). The value of (N_{neigh}) is a function of the r^c and particle volume fraction ϕ and may also vary for each particle in the suspension. For example, given that $\phi = 0.45$ and $r^c = 3.0$, the average value of N_{neigh} is found to be 6.

For the semi-implicit scheme, the total number of operations involved in computing the velocities (line 4 and 5) is therefore found to be $(142N \times N_{neigh}) \times N_{sweep})$. On the other hand, the total count for the explicit algorithm (line 4 to 15) is given by $(113N \times N_{neigh} + 6N) \times N_{sub}$. Here, N_{sub} is the number of sub-time steps requiblack by the explicit algorithm relative to the semi-implicit. Taking $N_{neigh} = 6$, the number of operations involved for the semi-implicit and explicit methods are therefore $(852N \times N_{sweep})$ and $(684N \times N_{sub})$ respectively. This implies that the efficacy of the semi-implicit approach depends on the number of sweeps N_{sweep} requiblack (which has been optimized to remain sufficiently small as previously discussed) in comparison with the number of sub-time step N_{sub} requiblack by the explicit approach. Therefore, the semi-implicit scheme would be faster as long as the condition $1.25N_{sweep} < N_{sub}$ holds.

4. Numerical results and discussion

In order to validate the proposed methodology, we simulate the simple shear test of a non-colloidal suspension and compare the pblackicted rheometric functions against some of the benchmark results. To demonstrate the efficiency of the proposed semi-implicit method over explicit schemes, we also simulate the same test with a Velocity-Verlet time integration scheme. For this test, a three dimensional computational box of size $32a \times 32a \times 32a$ is consideblack. Here, a is the radius of the suspended particle. While the top and bottom surfaces of the box are consideblack to be bounded by walls, the rest of the boundary surfaces

line	explicit	count	semi-implicit	count
1	DO $\alpha = 1$, N-1		DO $\alpha = 1$, N-1	
2	DO $\beta = \alpha$+1,N		DO $\beta = \alpha$+1, N	
3	IF $(s_{\alpha\beta} < r^c)$	6	IF $(s_{\alpha\beta} < r^c)$	6
4	$F_{\alpha\beta}$ = Eq. (1)	55	Integrate Eqs. (1),	142
5	$F_\alpha += F_{\alpha\beta}$	1	(2) and (3) implicitly	
6	$F_\beta -= F_{\alpha\beta}$	1	ENDIF	
7	$T_\alpha +=$ Eq. (2)	46	ENDDO	
8	$T_\beta +=$ Eq. (3)	4	ENDDO	
9	ENDIF			
10	ENDDO			
11	ENDDO			
12	DO $\alpha = 1$, N			
13	$V_\alpha += F_\alpha \Delta t / m_\alpha$	3		
14	$\omega_\alpha += T_\alpha \Delta t / I_\alpha$	3		
15	ENDDO			
Total		119		148

Table 1: The computational operations involved in the explicit integration of the lubrication force and torque are compablack against the proposed semi-implicit approach.

are assumed to be periodic. The top and bottom walls are moved at a constant but opposite velocities along the $x - axis$ determined from the prescribed input shear rate $\dot{\gamma}_{in}$. Due to the presence of wall slip at large particle volume fractions, the effective shear rate $\dot{\gamma}^e_{in}$ in the computational domain is calculated by interpolating the particles' velocities in the bulk. The schematic of the problem setup is shown in Fig. 3.

The configuration of the suspended particles inside the problem domain is setup using a Monte-Carlo approach. Based on the supplied value of r^c, an efficient linked-list algorithm is employed to determine the neighbor particles. Notice that r^c is not a free parameter and has to be less than $4a$. In order to regularize the singular nature of the lubrication forces, a parameter denoted as r^δ is specified. For inter-particle separations below the prescribed

value of r^{δ}, the lubrication force and torque are kept constant. Similar to previous studies [30, 31], the parameter r^{δ} is set a typical value of $0.001a$. The repulsion force parameters F_0 and τ are set as 8.4318×10^{-3} and 10^3 respectively. For dynamically adapting the N_{sweep}, its maximum value is set as 1024 and the tolerance parameter ϵ is set as 10^{-3}. Unless otherwise stated, the default dimensionless time step size Δt is typically set as 10^{-4} with the reference or characteristic time scale taken to be $t_{ref} = \dot{\gamma}^{-1}$. For simulations with explicit integration, the following version of Velocity-Verlet algorithm [32, 33] was employed.

$$
\begin{aligned}
\boldsymbol{r}_{\alpha}(t+\Delta t) &= \boldsymbol{r}_{\alpha}(t) + \Delta t \boldsymbol{V}_{\alpha}(t) + \frac{1}{2}\frac{(\Delta t)^2}{m}\boldsymbol{F}_{\alpha}(t) \\
\boldsymbol{V}^{*}_{\alpha}(t+\Delta t) &= \boldsymbol{V}_{\alpha}(t) + \lambda\frac{\Delta t}{m}\boldsymbol{F}_{\alpha}(t) \\
\boldsymbol{\omega}^{*}_{\alpha}(t+\Delta t) &= \boldsymbol{\omega}_{\alpha}(t) + \lambda\frac{\Delta t}{I}\boldsymbol{T}_{\alpha}(t) \\
\boldsymbol{F}_{\alpha}(t+\Delta t) &= \boldsymbol{F}_{\alpha}(\boldsymbol{r}(t+\Delta t), \boldsymbol{V}^{*}(t+\Delta t), \boldsymbol{\omega}^{*}(t+\Delta t)) \\
\boldsymbol{T}_{\alpha}(t+\Delta t) &= \boldsymbol{T}_{\alpha}(\boldsymbol{r}(t+\Delta t), \boldsymbol{V}^{*}(t+\Delta t), \boldsymbol{\omega}^{*}(t+\Delta t)) \\
\boldsymbol{V}_{\alpha}(t+\Delta t) &= \boldsymbol{V}_{\alpha}(t) + \frac{1}{2}\frac{\Delta t}{m}(\boldsymbol{F}_{\alpha}(t) + \boldsymbol{F}_{\alpha}(t+\Delta t)) \\
\boldsymbol{\omega}_{\alpha}(t+\Delta t) &= \boldsymbol{\omega}_{\alpha}(t) + \frac{1}{2}\frac{\Delta t}{I}(\boldsymbol{T}_{\alpha}(t) + \boldsymbol{T}_{\alpha}(t+\Delta t))
\end{aligned}
\tag{31}
$$

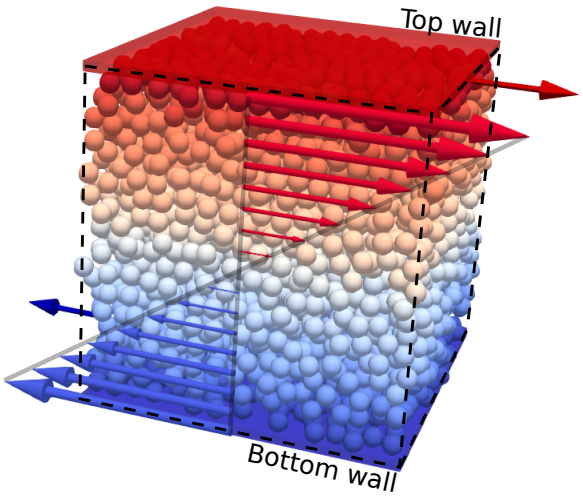

Figure 3: Schematic of the simple shear test. A cubic domain of side $32a$ is filled with mono-dispersed suspension of particles. The radius of the particles are set as $a = 1$ unit. As depicted, the shearing flow in the domain is established by moving the top and bottom walls at a constant speed in opposite directions along the $x - axis$. The periodic boundaries are marked in dashed lines.

Here, $\boldsymbol{F}_\alpha$ and $\boldsymbol{T}_\alpha$ denotes the total force and total torque on a given particle, $\boldsymbol{V}^*_\alpha$ and $\boldsymbol{\omega}^*_\alpha$ are the pblackicted translational and angular velocities and the parameter λ is set as 0.5.

4.1. Sensitivity of the semi-implicit approach to various parameters

To begin with, we carry out simulations to analyze the sensitivity of the results obtained to the choice of the r^c. As the rheometric functions are determined from the stresses in the particle system, the lubrication forces acting on the suspension particles need to be accurately resolved. In this regard, the value of r^c needs to be set sufficiently large to accurately take into account the inter-particle lubrication forces. As a first choice we set r^c as $2.5a$ and simulated the simple shear test for different particle volume fraction ranging from 0.05 to 0.48. The non-dimensional input shear rate $\dot{\gamma}^*_{in}$, defined as $\frac{6\pi\eta\bar{a}^2\dot{\gamma}^e_{in}}{F_0}$ which determines the relative strength of the viscous force to the repulsion force, is set as 250. Here, $\bar{a}$ is defined as $\frac{a_\alpha a_\beta}{a_\alpha+a_\beta}$. For the mono-dispersed system of spherical neutrally-buoyant particles of radius $a = 1$ and density $\rho_p = 1$ consideblack in this study, the values of particles' mass and moment of inertia are set as $\frac{4\pi}{3}$ and $\frac{8\pi}{15}$ respectively. The simulation parameters are set such that the particle Reynolds number $Re_p = \frac{\rho_f a^2\dot{\gamma}_{in}}{\eta}$ is very low with a value of 0.00625 and therefore the effects of inertial motion of the particles on the suspension rheology should be insignificant. Very high values of ϕ were not consideblack as disorder-to-order transition might occur and contact frictional forces would be significant [28]. Using the position of the particles and the inter-particle forces, the stress tensor in the bulk region was continuously monitoblack via the Irving-Kirkwood method [34] as follows:

$$\boldsymbol{\sigma} = -\frac{1}{V}\left(\sum_\alpha m_\alpha \mathbf{v}_\alpha \mathbf{v}_\alpha + \frac{1}{2}\sum_{\alpha\neq\beta}\mathbf{r}_{\alpha\beta}\mathbf{F}_{\alpha\beta}\right), \tag{32}$$

where, V is the volume of the bulk region, $\mathbf{v}$ is the perturbation velocity vector, $\mathbf{r}_{\alpha\beta} = \mathbf{r}_\alpha - \mathbf{r}_\beta$ is the relative position vector of a α particle with respect to its β neighbor particle and $\mathbf{F}_{\alpha\beta}$ is the inter-particle force vector. It should be pointed out that ordering of particles can occur near the walls which grows with particle concentration. For the values of ϕ simulated in this study, the layering of particles near the wall was observed to less significant. Moreover, the Irving-Kirkwood method is applied only on the bulk region that is sufficiently far away from the walls. Therefore, the steric effects of the walls on the pblackicted rheology is negligible.

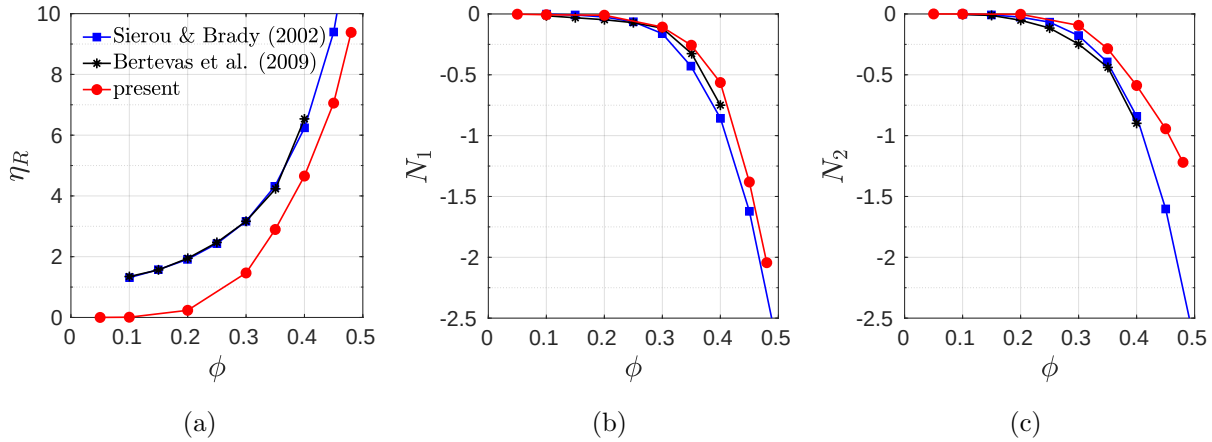

Figure 4: The variation of a) the suspension relative viscosity and the normal stress differences b) N1 and c) N2 with the particle concentration obtained with $r^c = 2.5a$.

Once the stresses reached a steady value, the relative viscosity of the suspension (η_R) and the dimensionless normal stress differences (N_1 & N_2) were estimated as defined below.

$$\eta_R = \frac{\sigma_{xz}}{\eta\dot{\gamma}} \; ; \; N_1 = \frac{\sigma_{xx} - \sigma_{zz}}{\eta\dot{\gamma}} \; ; \; N_2 = \frac{\sigma_{zz} - \sigma_{yy}}{\eta\dot{\gamma}} \tag{33}$$

The pblackicted rheometric functions of the suspension obtained for $r^c = 2.5a$ are shown in Fig. 4. For comparison purpose, the results of Sierou and Brady [28] and Bertevas et al. [35] have been co-plotted. Although there is a good qualitative match, a clear underestimation of the suspension relative viscosity and the non-dimensional normal stress differences with respect to the reference results is observed. Results tested with different choices of Δt and r^δ did not show any appreciable differences. As expected, a sharp decrease in the suspension relative viscosity with particle volume fraction is also noticeable. This is due to the declining neighbor contribution at lower particle volume fractions which in turn results in vanishing stresses in the bulk.

The underestimation of the suspension properties clearly indicated the insufficient contribution from the neighbor particles. Therefore, another set of simulation were conducted with $r^c = 3a$. The results of the simulations are shown in Fig. 5. With the increase in the value of r^c, the pblackicted results can be found to be in excellent agreement with the reference results. Especially for $\phi > 0.30$, the pblackicted suspension relative viscosity was

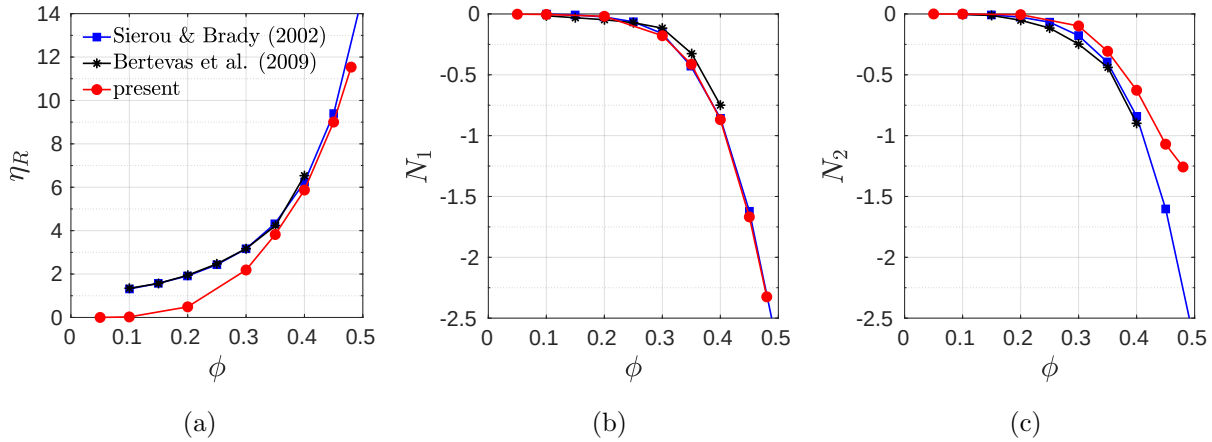

Figure 5: Variation of a) the suspension relative viscosity and the normal stress differences b) N1 and c) N2 with the particle concentration. Results corresponds to simulations with $r^c = 3a$.

found to match well the results of Sierou and Brady [28]. This implies that upon tunning of the parameter r^c, the current methodology is well suited for estimating the rheological properties of dense suspensions. While the $N1$ normal stress difference is found to be accurately pblackicted, the values of $N2$ remained slightly underestimated, but still in line to those reported in Ref. [28].

In search of avenues to speed-up the calculations, the effect of blackucing the box size from 32^3a^3 to 16^3a^3 was studied. Although, there was an obvious speedup in the calculation,

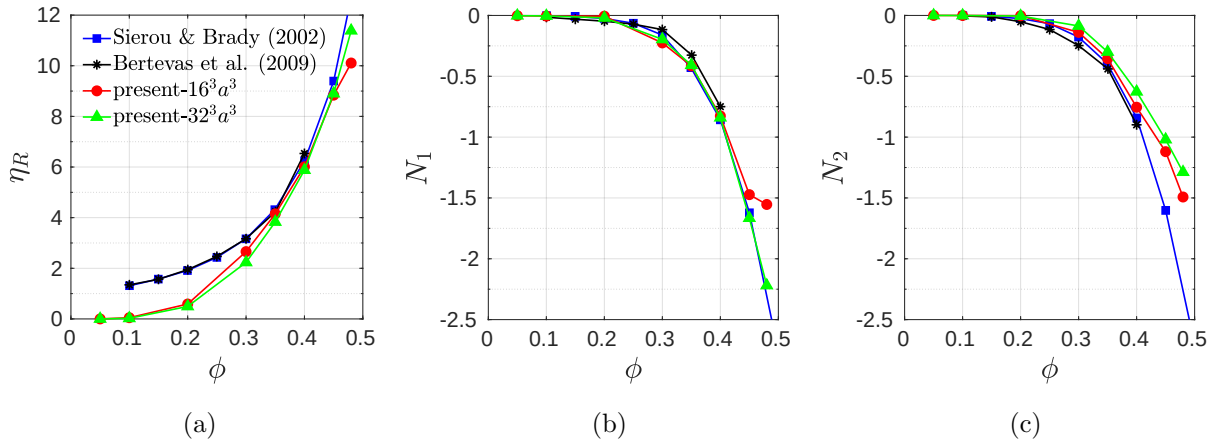

Figure 6: Comparison of results obtained with cubic domains of side $16a$ and $32a$. Variation of the rheometric functions with particle concentration.

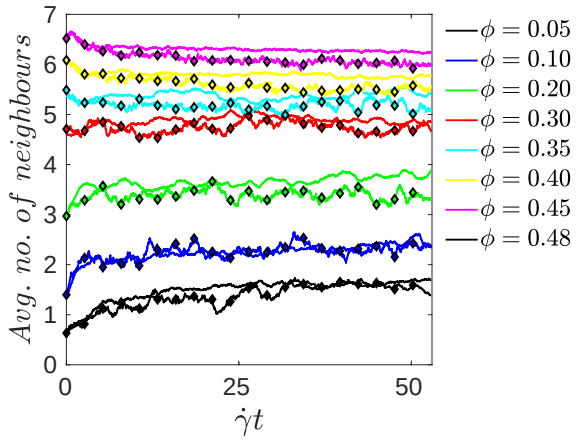

Figure 7: Comparison of the average number of neighbors for box sizes 16^3a^3 (line with $\Diamond$) and 32^3a^3 (line).

the results obtained were relatively less accurate. For the two different box sizes consideblack, Table 2 compares the number of suspended particles in the domain and the time taken to simulate upto $\dot{\gamma}t = 52.8$. It can be noticed that with almost an order of magnitude decrease in the number of particles, the simulations using the 16^3a^3 box is at least seven times faster than

ϕ	16^3a^3		32^3a^3	
	N	run time	N	run time
0.05	49	0.19(8.79x)	391	1.67
0.10	98	0.74(6.49x)	782	4.80
0.20	196	1.92(8.05x)	1565	15.47
0.30	294	4.16(7.48x)	2347	31.12
0.35	343	4.49(9.05x)	2738	40.64
0.40	392	5.65(8.79x)	3129	49.68
0.45	441	7.51(8.08x)	3520	60.75
0.48	470	8.34(8.42x)	3755	70.29

Table 2: For the two box sizes consideblack, time taken (in hours) by the semi-implicit and explicit integration schemes to reach $\dot{\gamma}t = 52.8$ is compablack. Here, N is the number of suspension particles in the domain. The values enclosed in brackets are the relative speed-up in calculations of smaller domain when compablack against the larger domain. All CPU-time data refer to single-core computations.

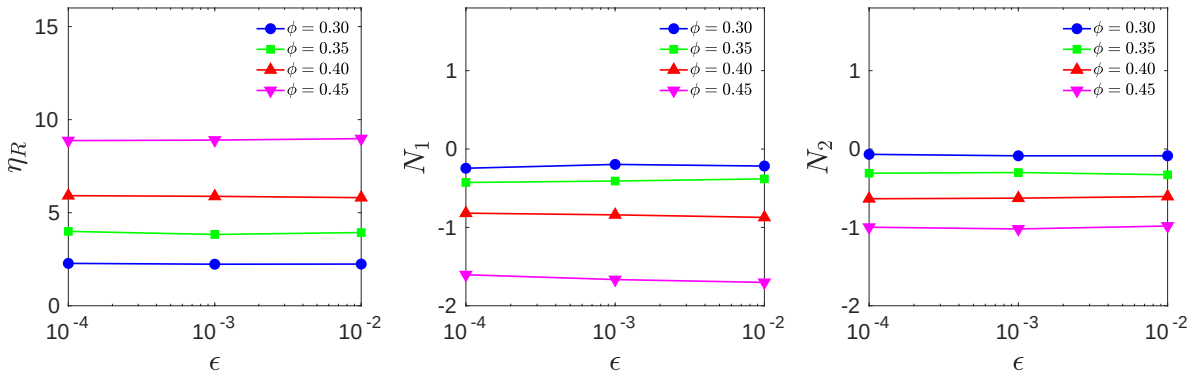

Figure 8: Convergence of the a) relative viscosity and normal stress differences b) N_1 and c) N_2 for different vales of ϕ and ϵ.

the 32^3a^3 box. Fig. 6 compares the viscometric functions obtained with the computational domain of size 16^3a^3 against 32^3a^3. With a blackuced box size, the results obtained are in good agreement with the reference results for a particular range of ϕ varying between 0.35 to 0.45. However, a considerable underestimation of the suspension relative viscosity is observed for $\phi < 0.35$ and $\phi > 0.45$. In a similar manner, the N_1 and N_2 normal stress differences are also found to somewhat underestimated at high particle volume fractions. Notice that the underestimation is observed despite the average number of neighbors (N_{neigh}^{avg}) being almost the same for both box sizes (see Fig. 7). These results clearly indicate the presence of box and possible confinement effects due to the choice of a realistic slit channel geometry. Hence, the larger domain with side of length $32a$ was used for all the simulations reported henceforth.

The accuracy and robustness of the semi-implicit integration are highly dependent on the tolerance parameter ϵ which controls the number of sweeps (N_{sweep}) requiblack at each step of the time integration. In order to assess the influence of the tolerance parameter on the pblackicted suspension rheology, simulations were carried out with $\epsilon = 10^{-2}, 10^{-3}$ and 10^{-4}. As seen from Fig. 8, irrespective of the particle concentration, the variation of the suspension relative viscosity and dimensional normal stress differences with ϵ is fairly low. This is attributed to the choice of the Δt (taken as 10^{-4}) being low enough to mask the effect

of ϵ. Hence, the present results indicate that a value of 10^{-3} should be sufficient to ensure that converged results are obtained.

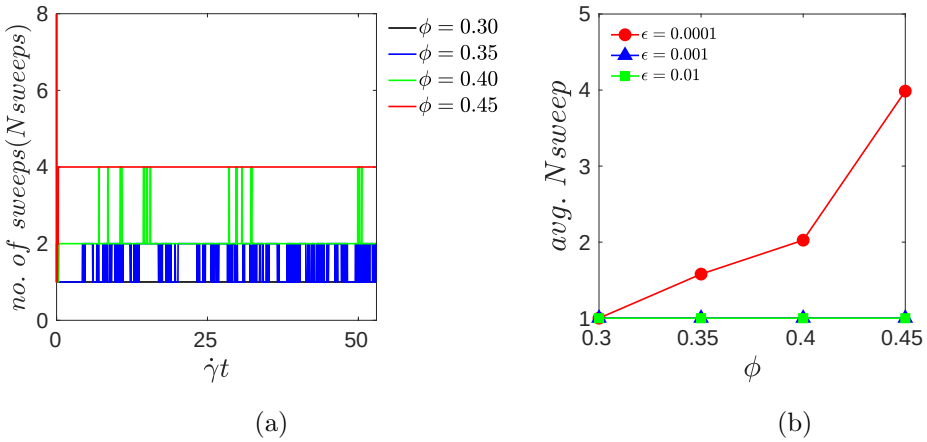

(a) (b)

Figure 9: Variation of number of sweeps (N_{sweep}) for a) $\epsilon = 0.0001$ and b) comparison of average number of sweeps N^{avg}_{sweep} for different ϕ and ϵ. For $\epsilon = 0.001$ and 0.01, the N_{sweep} remained as 1 throughout the simulation.

It is pointed out that employing a sufficiently low value of ϵ is necessary to avoid unnecessary increase in the number of sweeps requiblack and in turn the computational cost. To emphasis this, for the different values of ϵ and ϕ studied, the variation of the N_{sweep} with time is shown in Fig. 9. While the value of N^{avg}_{sweep} remains as 1 for $\epsilon = 10^{-2}$ and 10^{-3} throughout the simulation, for $\epsilon = 10^{-4}$, it often increases from 2 to 4 depending on the particle volume fraction. To explain the dependency of the N_{sweep} on the particle concentration, the average number of sweeps N^{avg}_{sweep} is also shown in Fig. 9b. As can be seen, the number of sweeps increases with particle concentration to accommodate for the corresponding decrease in the average inter-particle separation. This clearly demonstrates the superior adaptive nature of the proposed algorithm to suit the dynamics of the problem, as well as, the accuracy demanded by the user. Such a feature also establish the robustness of the proposed algorithm to solve problems with varying degree of numerical complexity.

4.2. Semi-implicit versus explicit integration

To demonstrate the efficacy of the proposed semi-implicit integration scheme, a comparative study against a typically employed explicit integration approach is presented in this

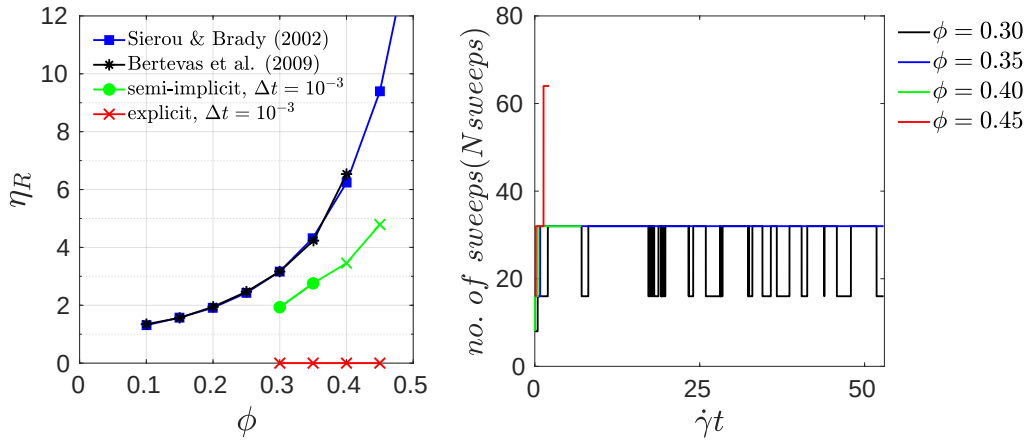

(a) (b)

Figure 10: a) Suspension relative viscosity pblackicted by the semi-implicit and explicit integration schemes with $\Delta t = 10^{-3}$ are compablack. Stable and unstable simulations are marked with filled circles and crosses respectively. b) Variation of the N_{sweep} parameter in the case of the semi-implicit scheme for different particle concentration.

section. To this end, the simple shear test was simulated by solving the Eqs. (1), (2) and (5) using a second order accurate Velocity-Verlet scheme. To compare the stability and accuracy of the schemes, both the explicit and the semi-implicit methods were tested for time step size varying from 10^{-3} to 10^{-6}. For the semi-implicit scheme, the convergence criterion ϵ and the maximum value for N_{sweep} were set as 10^{-3} and 1024 receptively.

For $\Delta t = 10^{-3}$, the simulations using the explicit scheme failed instantly at $\dot{\gamma}t = 0$ for the range of volume fraction studied. On the other hand, for the same time step size, the semi-implicit scheme was able to simulate particle volume fractions up to 0.35 through dynamic adaption of the N_{sweep} parameter. Although after reaching the steady state, the simulations ended prematurely due to particle-overlapping at $\dot{\gamma}t = 7.1$ and $\dot{\gamma}t = 2.2$ for $\phi = 0.40$ and $\phi = 0.45$ respectively. Fig. 10a shows suspension relative viscosity pblackicted by the semi-implicit and the explicit scheme. The stable and unstable simulations are marked with filled circles and crosses respectively. In Fig. 10b, corresponding variation of the N_{sweep} parameter for the semi-implicit scheme is shown. Although, the presented algorithm systematically increases the N_{sweep} with ϕ, the inter-particle forces from the lubrication and repulsion was insufficient to maintain the excluded volume effect of the particles. This is partially attributed

to the choice of r^{δ} which limits the maximum lubrication force on a particle-pair and partially to the explicit integration of the repulsion force term. It was found that blackucing the r^{δ} to lower values, say 10^{-4}, indeed provided stable simulations for $\phi > 0.35$. On the other hand, it should be noted that the explicit scheme is unstable for all volume fractions when $\Delta t = 10^{-3}$.

By lowering the value of Δt to 10^{-4}, a marked improvement on the accuracy as well as stability of the semi-implicit scheme was observed. Fig. 11 shows the variation in the relative viscosity of the suspension with particle volume fraction. The pblackictions of the proposed semi-implicit approach can be found to be in good agreement with the reference data. On the other hand, with $\Delta t = 10^{-4}$, the explicit scheme showed a clear underestimation of the suspension relative viscosity and also failed to run for $\phi \geq 0.45$. Upon decreasing the Δt to 10^{-5}, the explicit scheme simulations were able to run stably at higher particle volume fractions, however, the pblackicted suspension relative viscosity were somewhat overestimated. To ensure the solution from the explicit scheme is independent of the time step size, another set of simulations were conducted with a further refined Δt equal to 10^{-6}. From Fig. 11, it can be noticed that the pblackictions of Δt equal to 10^{-5} and 10^{-6} almost overlap each other, indicating the absence of any significant improvement on the pblackiction of the suspension relative viscosity. Comparing these results, it is evident that the proposed semi-implicit

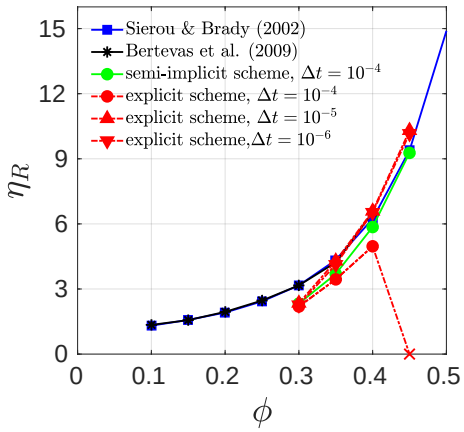

Figure 11: Suspension relative viscosity pblackicted by the semi-implicit and explicit integration schemes (with different time step size) are compablack. Stable and unstable simulations are marked with filled circles and crosses respectively.

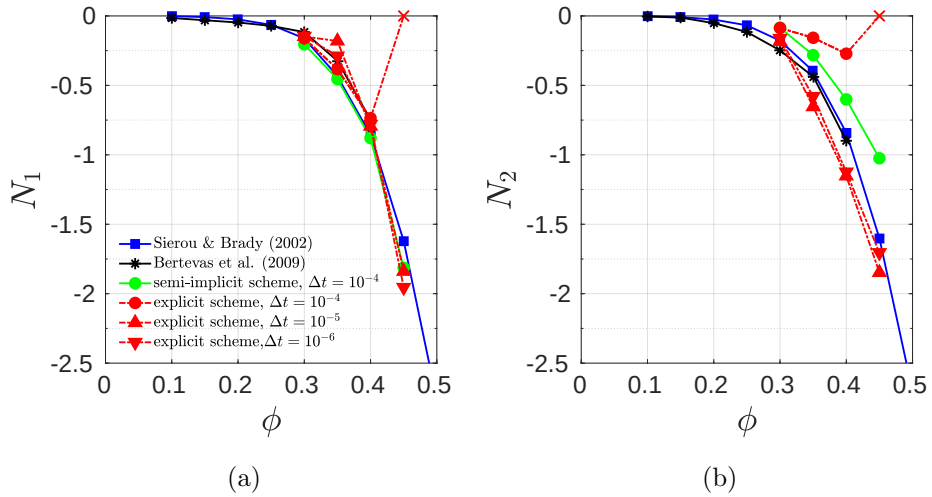

(a) (b)

Figure 12: Dimensionless normal stress differences pblackicted by the semi-implicit and explicit integration schemes.

approach is capable of stably simulating the test even at higher time step size. Moreover, compablack to the explicit scheme, the pblackicted suspension relative viscosities were in much better agreement with the reference data. Similar observations could also be made from Fig. 12 in which the variation of the dimensionless normal stress differences pblackicted by the semi-implicit and the explicit method are compablack.

To further elaborate on the simulation speed-up gained by using the semi-implicit scheme, the time taken by the semi-implicit and the explicit integration schemes to simulate the simple shear test are compablack. To determine the actual speed-up, it is necessary to take into account the accuracy of the results obtained from both methods. For this purpose, Fig. 13 compares the relative viscosity of the suspension at $\phi = 0.40$ pblackicted by the semi-implicit and the explicit methods with different time step sizes. The stable and unstable simulation are again marked with filled circles and crosses respectively. It can be observed that both the explicit scheme and semi-implicit schemes are unstable for $\Delta t = 10^{-3}$. For $\Delta t = 10^{-4}$ both schemes were found to be stable, however, the semi-implicit scheme was found to be more accurate. Moreover, unlike the semi-implicit scheme, the explicit scheme with $\Delta t = 10^{-4}$ was also found to be unstable for the case of $\phi = 0.45$,. With reference to the results of Sierou and Brady [28], the error in the pblackicted relative viscosity of the suspension was 6% and

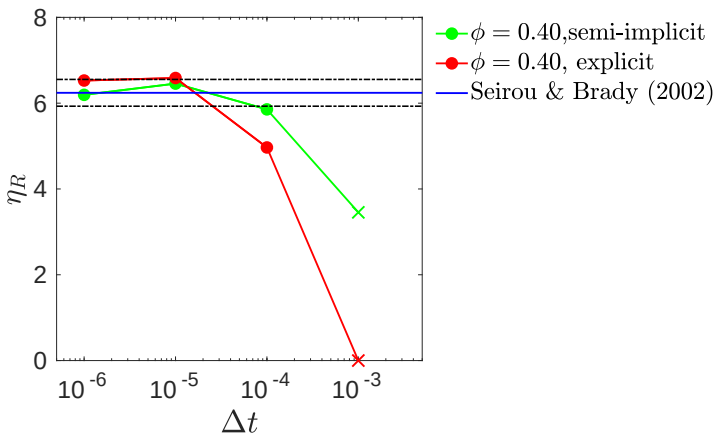

Figure 13: Suspension relative viscosity pblackicted by the semi-implicit and explicit integration schemes for $\phi = 0.40$ are compablack.

20% for the semi-implicit and explicit schemes. Upon further decrease of the time step size, the converged value of the suspension viscosity pblackicted by the explicit scheme was within 6% error margin from the reference value. On the other hand, the semi-implicit scheme was able to pblackict the suspension viscosity with less than 0.01% error. Based on comparable accuracy levels (i.e close to 5%) results, the time taken to simulate with $\Delta t = 10^{-4}$ for the semi-implicit scheme and $\Delta t = 10^{-5}$ for the explicit scheme are compablack to assess the performance of the two schemes.

Table 3 shows the time taken by the semi-implicit and the explicit integration schemes to

N	ϕ	Semi-implicit integration		explicit integration - run time		
		N_{sweep}^{avg}	run time $\Delta t = 10^{-4}$	$\Delta t = 10^{-4}$ $N_{sub} = 1$	$\Delta t = 10^{-5}$ $N_{sub} = 10$	$\Delta t = 10^{-6}$ $N_{sub} = 100$
2347	0.30	1	7.22	2.54	44.75	285.60
2738	0.35	1	9.61	3.99	60.40	365.48
3129	0.40	1	11.90	4.62	70.44	425.25
3520	0.45	1	14.32	-	81.70	563.10

Table 3: Time take, in hours, by the semi-implicit and explicit time-integration schemes to reach $\dot{\gamma}t = 10.56$ are compablack.

simulate the simple shear test for $\dot{\gamma}t = 10.56$. The average number of sweeps N_{sweep}^{avg} for the semi-implicit schemes can be compablack to the number of explicit sub-time-step calculated as $N_{sub} = \Delta t_{eqiv}/\Delta t$, where $\Delta t_{eqiv} = \Delta t/N_{sweep}^{avg}$ is the equivalent semi-implicit time step size, for insights into the relative computing complexity of the approaches. For the chosen value of $\epsilon = 10^{-3}$ in the case of the semi-implicit scheme, the N_{sweep}^{avg} remained as 1 for the range of ϕ that were simulated. Hence, the value of N_{sub} for Δt equal to 10^{-4}, 10^{-5} and 10^{-6} can be found to be $1, 10$ and 100 respectively. As previously shown in Sec. 3.1, the condition under which the semi-implicit scheme can exhibit potential speed-up in calculations is $1.25N_{sweep} < N_{sub}$. In accordance with this condition, it can be found from the Table 3 that for $\Delta t = 10^{-4}$, the explicit scheme is slightly faster than the semi-implicit scheme. However, for $\Delta t = 10^{-5}$ and 10^{-6}, the corresponding value of N_{sub} is significantly lower than the N_{sweep}^{avg} and therefore a drastic speed-up in calculations is observed. In fact, the observed speed-up with respect to the explicit scheme scales roughly between 0.4 to $0.6N_{sub}$. It is necessary to point out that the above analysis is independent of the simulation box size as the N_{sweep}^{avg} and the N_{neigh}^{avg} does not increase with box size.

5. Summary and Conclusion

To summarize, this work presents a new lubrication dynamics method suitable for simulation of concentrated non-Brownian particulate systems with a Newtonian matrix. This method exploits the dominance of short-range lubrication interactions over long-range hydrodynamic interactions in dense particle systems to employ a minimalistic model to pblackict the rheometric functions of non-colloidal suspensions. In addition to the lubrication forces, a short-range inter-particle repulsive force is consideblack to simulate the finite inter-particle separations, e.g. due to surface roughness, in realistic systems. Another feature of the proposed method is the inclusion of particles' rotational effects in a conservative pairwise form. The most important aspect of the method is the semi-implicit splitting integration scheme that enables stable and accurate simulation to be carried out in a fast manner. The presented pairwise semi-implicit procedure allows small system of equations to be generated for each particle-pair which can be solved analytically to compute the particles' linear and angular velocities. Using a pblackefined tolerance to control the accuracy and computational cost,

the iterative semi-implicit scheme uses a dynamic adaptation algorithm to keep the number of iterations (N_{sweep}) sufficiently small. In brief, the proposed methodology, besides enjoying the full conservation of the system's linear and angular momentum, is configublack to be simple and efficient.

The validation of the proposed model was carried-out using a simple shear test to estimate the rheometric functions a non-colloidal suspension with a Newtonian matrix. The pblackicted suspension relative viscosity and normal stress differences were in excellent agreement with the benchmark results available from open literature. The influence of various simulation parameters on the pblackicted suspension properties was systematically studied and discussed. To demonstrate the speed-up in the calculations, the performance of the semi-implicit method was compablack against the Velocity-Verlet scheme. With due consideration to the accuracy and stability, the presented semi-implicit splitting integration scheme was shown to be significantly faster than the Velocity-Verlet scheme. The dynamically adapted pairwise iterative scheme allows the proposed methodology to employ relatively larger time steps which substantially blackuces the simulation durations. Moreover, at higher volume fractions in particular, the semi-implicit scheme is found to be relatively more stable than the explicit Velocity-Verlet scheme. It was also observed that, for the present methodology to be simultaneously accurate and fast, the N_{sweep} parameter has to be sufficiently small. This requires a careful choice of the tolerance parameter ϵ and the time step size Δt. For fast calculations higher Δt and lower ϵ, and for better accuracy lower Δt with higher ϵ is recommended. The present scheme can be used to simulate dense complex suspensions, e.g. particles suspended in a non-Newtonian media, by adopting new equations of lubrication forces for shear-thinning and thickening liquids [21, 22, 23] which is the current focus of research.

6. Acknowledgements

This research is supported by the Basque Government through the BERC 2018-2021 program and by the Spanish State Research Agency through BCAM Severo Ochoa excellence accblackitation SEV-2017-0718 and through project RTI2018-094595-B-I00 funded by (AEI/FEDER, UE) and acronym VIRHACOST. Financial support received from MATHEO,

a project funded by the Basque Business Development Agency under ELKARTEK 2019 program (grant KK-2019/00085) is also gratefully acknowledged.

7. Appendix A: Modeling of the wall boundaries

The interaction of one suspended particle with the top and bottom wall surfaces is modeled as an extra pair equation. In this sense, the wall is treated as any other particle with a different interaction. When a spherical particle of radius a moving with velocity $\boldsymbol{V}$ is within the cut-off distance from a wall moving at velocity $\boldsymbol{V}_w$, the normal and tangential forces exerted on the suspension particle are calculated based on Cox and Brenner [36] and Goldman et al. [37] as,

$$\begin{aligned} \boldsymbol{F}^n_{\alpha w} &= f_{\alpha w}(\boldsymbol{V}_\alpha - \boldsymbol{V}_w)\cdot \boldsymbol{e}_{\alpha w}\boldsymbol{e}_{\alpha w} \\ \boldsymbol{F}^t_{\alpha w} &= g_{\alpha w}(\boldsymbol{V}_\alpha - \boldsymbol{V}_w)\cdot (\boldsymbol{1} - \boldsymbol{e}_{\alpha w}\boldsymbol{e}_{\alpha w}) \end{aligned} \tag{34}$$

where

$$\begin{aligned} f_{\alpha w} &= -6\pi\eta a\left\{\frac{a}{h} + \frac{1}{5}ln\left(\frac{a}{h}\right) + k\right\} \\ g_{\alpha w} &= -\frac{16}{5}\pi\eta a\ \ln\left(\frac{a}{h}\right) \end{aligned} \tag{35}$$

Here, k is a suitable constant taken as 0.971264. To solve for the particle velocity using the semi-implicit scheme, for every particle-wall pair, their final velocities $\tilde{\boldsymbol{V}}_\alpha$ are written in terms of the previous velocities $\boldsymbol{V}'_\alpha$ as

$$\tilde{\boldsymbol{V}}_\alpha = \boldsymbol{V}'_\alpha + \tilde{\boldsymbol{F}}_{\alpha w}\frac{\Delta t_{sweep}}{m_\alpha} \tag{36}$$

$$\tilde{\boldsymbol{V}}_w = \boldsymbol{V}'_w = \boldsymbol{V}_w \tag{37}$$

Subtracting Eqs. (36) and (37), and substituting Eq. (34), we get

$$\tilde{\boldsymbol{V}}_{\alpha w}\cdot\left\{(g_{\alpha w} - f_{\alpha w})\,\boldsymbol{e}_{\alpha w}\boldsymbol{e}_{\alpha w} + (1 - g_{\alpha w})\boldsymbol{1}\right\}\frac{\Delta t_{sweep}}{m_\alpha} = \boldsymbol{V}'_{\alpha w} \tag{38}$$

for which the solution is

$$\tilde{\boldsymbol{V}}_\alpha = \boldsymbol{V}_w + \left(\frac{1}{1 - B_{\alpha w}}\right)\boldsymbol{V}'_{\alpha w}\cdot\left\{\boldsymbol{1} + \left(\frac{A_{\alpha w} - B_{\alpha w}}{1 - B_{\alpha w}}\right)\boldsymbol{e}_{\alpha w}\boldsymbol{e}_{\alpha w}\right\} \tag{39}$$

where

$$\begin{aligned} A_{\alpha w} &= f_{\alpha w}\Delta t_{sweep}/m_\alpha \\ B_{\alpha w} &= g_{\alpha w}\Delta t_{sweep}/m_\alpha. \end{aligned} \tag{40}$$

8. Appendix B: A generalised formalism analogous to Stokesian Dynamics

In this study, a pairwise semi-implicit approach to simulate dense suspensions with Newtonian matrices in the Stokes regime is presented. Although, this iterative procedure is completely different from the standard SD approach, herein, we present briefly an equivalent SD system to solve. The general SD formalism for a force-free torque-free particle system suspended in an ambient linear flow in Stokes regime is as follows.

$$\begin{bmatrix} \mathbf{R}_{FU} & \mathbf{R}_{F\Omega} & \mathbf{R}_{FE} \\ \mathbf{R}_{TU} & \mathbf{R}_{T\Omega} & \mathbf{R}_{TE} \\ \mathbf{R}_{SU} & \mathbf{R}_{S\Omega} & \mathbf{R}_{SE} \end{bmatrix} \cdot \begin{pmatrix} \mathbf{U} - \mathbf{U}^{\infty} \\ \mathbf{\Omega} - \mathbf{\Omega}^{\infty} \\ -\mathbf{E}^{\infty} \end{pmatrix} + \begin{pmatrix} \mathbf{f} \\ \mathbf{t} \\ \mathbf{0} \end{pmatrix} = \begin{pmatrix} \mathbf{F} \\ \mathbf{T} \\ \mathbf{S} \end{pmatrix} = \begin{pmatrix} \mathbf{0} \\ \mathbf{0} \\ \mathbf{S} \end{pmatrix} \tag{41}$$

Here, $\mathbf{R}$ is the resistance tensor, $\mathbf{U}$ and $\mathbf{U}^{\infty}$ are the particle and ambient fluid velocities respectively, $\mathbf{\Omega}$ is the particle angular velocity, $\mathbf{\Omega}^{\infty}$ is the fluid vorticity, $\mathbf{E}^{\infty}$ is the strain-rate tensor, $\mathbf{f}$ and $\mathbf{t}$ are the non-hydrodynamic contribution towards the particles' total force $\mathbf{F}$ and torque $\mathbf{T}$ respectively. In a simple shear flow, the particle motion can be solved as

$$\mathbf{U} - \mathbf{U}^{\infty} = \mathbf{R}_{FU}^{-1} \cdot [\mathbf{f} + \mathbf{R}_{FE} : \mathbf{E}^{\infty}] \tag{42}$$

$$\mathbf{\Omega} - \mathbf{\Omega}^{\infty} = \mathbf{R}_{TU}^{-1} \cdot [\mathbf{t} + \mathbf{R}_{TE} : \mathbf{E}^{\infty}] \tag{43}$$

For fast simulation of dense systems, whose rheology is dominated by the inter-particle lubrication forces, the interaction of the particles with the background flow field is neglected ($\mathbf{E}^{\infty} \rightarrow \mathbf{U}^{\infty} = \Omega^{\infty} = 0$). In the absence of a background flow, the particles are driven by its interaction with moving boundaries ($\mathbf{f}_b, \mathbf{t}_b$) and amongst particles in the proposed lubrication dynamics model. Considering these and employing the pairwise lubrication forces/torques, derived from the solution of the Stokes flow problem, in a quasi-static, non-zero inertia approach to compute particle acceleration, the equivalent SD system is obtained by rewriting Eq. 41 as follows.

$$\begin{bmatrix} \mathbf{R}_{FU} & \mathbf{R}_{F\Omega} \\ \mathbf{R}_{TU} & \mathbf{R}_{T\Omega} \end{bmatrix} \cdot \begin{pmatrix} \mathbf{U} \\ \mathbf{\Omega} \end{pmatrix} + \begin{pmatrix} \mathbf{f} \\ \mathbf{t} \end{pmatrix} + \begin{pmatrix} \mathbf{f}_b \\ \mathbf{t}_b \end{pmatrix} = \begin{pmatrix} m\dot{\mathbf{U}} \\ I\dot{\mathbf{\Omega}} \end{pmatrix} \tag{44}$$

References

[1] J. Mewis, N. J. Wagner, Colloidal Suspension Rheology, Cambridge Series in Chemical Engineering, Cambridge University Press, 2011. doi:10.1017/CBO9780511977978.

[2] I. Frigaard, Simple yield stress fluids, Current Opinion in Colloid & Interface Science 43 (2019) 80 – 93, rheology. doi:https://doi.org/10.1016/j.cocis.2019.03.002.
URL http://www.sciencedirect.com/science/article/pii/S1359029419300068

[3] R. I. Tanner, Review: Rheology of noncolloidal suspensions with non-Newtonian matrices, Journal of Rheology 63 (4) (2019) 705–717. arXiv:https://doi.org/10.1122/1.5085363, doi:10.1122/1.5085363.
URL https://doi.org/10.1122/1.5085363

[4] J. F. Brady, G. Bossis, Stokesian Dynamics, Annual Review of Fluid Mechanics 20 (1) (1988) 111–157. arXiv:https://doi.org/10.1146/annurev.fl.20.010188.000551, doi:10.1146/annurev.fl.20.010188.000551.
URL https://doi.org/10.1146/annurev.fl.20.010188.000551

[5] A. Sierou, J. F. Brady, Accelerated Stokesian Dynamics simulations, Journal of Fluid Mechanics 448 (2001) 115146. doi:10.1017/S0022112001005912.

[6] R. C. Ball, J. R. Melrose, A simulation technique for many spheres in quasi-static motion under frame-invariant pair drag and Brownian forces, Physica A: Statistical Mechanics and its Applications 247 (1997). doi:10.1016/s0378-4371(97)00412-3.

[7] A. Kumar, J. J. L. Higdon, Origins of the anomalous stress behavior in charged colloidal suspensions under shear, Phys. Rev. E 82 (2010) 051401. doi:10.1103/PhysRevE.82.051401.
URL https://link.aps.org/doi/10.1103/PhysRevE.82.051401

[8] G. S. Bolintineanu, D. S.and Grest, J. B. Lechman, F. Pierce, S. J. Plimpton, P. R. Schunk, Particle dynamics modeling methods for colloid suspensions, Computational Particle Mechanics 1 (3) (2014) 321–356. doi:10.1007/s40571-014-0007-6.
URL https://doi.org/10.1007/s40571-014-0007-6

[9] W. R. Hwang, M. A. Hulsen, H. E. Meijer, Direct simulations of particle suspensions in a viscoelastic fluid in sliding bi-periodic frames, Journal of Non-Newtonian Fluid Mechanics 121 (1) (2004) 15 – 33. doi:https://doi.org/10.1016/j.jnnfm.2004.03.008.
URL http://www.sciencedirect.com/science/article/pii/S0377025704000655

[10] G. D'Avino, P. Maffettone, M. Hulsen, G. Peters, A numerical method for simulating concentrated rigid particle suspensions in an elongational flow using a fixed grid, Journal of Computational Physics 226 (1) (2007) 688 – 711. doi:https://doi.org/10.1016/j.jcp.2007.04.027.
URL http://www.sciencedirect.com/science/article/pii/S0021999107002021

[11] A. Wachs, A. Hammouti, G. Vinay, M. Rahmani, Accuracy of finite volume/staggered grid distributed Lagrange multiplier/fictitious domain simulations of particulate flows, Computers & Fluids 115 (2015) 154 – 172. doi:https://doi.org/10.1016/j.compfluid.2015.04.006.
URL http://www.sciencedirect.com/science/article/pii/S0045793015001152

[12] S. Krishnan, E. S. Shaqfeh, G. Iaccarino, Fully resolved viscoelastic particulate simulations using unstructured grids, Journal of Computational Physics 338 (2017) 313 – 338. doi:https://doi.org/10.1016/j.jcp.2017.02.068.
URL http://www.sciencedirect.com/science/article/pii/S0021999117301717

[13] A. R. Koblitz, S. Lovett, N. Nikiforakis, Direct numerical simulation of particle sedimentation in a Bingham fluid, Phys. Rev. Fluids 3 (2018) 093302. doi:10.1103/PhysRevFluids.3.093302.
URL https://link.aps.org/doi/10.1103/PhysRevFluids.3.093302

[14] N. Trask, M. Maxey, K. Kim, M. Perego, M. L. Parks, K. Yang, J. Xu, A scalable consistent second-order SPH solver for unsteady low Reynolds number flows, Computer Methods in Applied Mechanics and Engineering 289 (2015) 155 – 178. doi:https://doi.org/10.1016/j.cma.2014.12.027.
URL http://www.sciencedirect.com/science/article/pii/S0045782514005064

[15] N. Trask, M. Maxey, X. Hu, Compact moving least squares: An optimization framework for generating high-order compact meshless discretizations, Journal of Computational Physics 326 (2016) 596 – 611. doi:https://doi.org/10.1016/j.jcp.2016.08.045.
URL http://www.sciencedirect.com/science/article/pii/S0021999116304028

[16] P. Polfer, T. Kraft, C. Bierwisch, Suspension modeling using smoothed particle hydrodynamics: Accuracy of the viscosity formulation and the suspended body dynamics, Applied Mathematical Modelling 40 (4) (2016) 2606 – 2618. doi:https://doi.org/10.1016/j.apm.2015.10.013.
URL http://www.sciencedirect.com/science/article/pii/S0307904X15006587

[17] A. Vázquez-Quesada, M. Ellero, Rheology and microstructure of non-colloidal suspensions under shear studied with smoothed particle hydrodynamics, Journal of Non-Newtonian Fluid Mechanics 233 (2016) 37 – 47, papers presented at the Rheology Symposium in honor of Prof. R. I. Tanner on the occasion of his 82nd birthday, in Vathi, Samos, Greece. doi:https://doi.org/10.1016/j.jnnfm.2015.12.009.
URL http://www.sciencedirect.com/science/article/pii/S0377025715002189

[18] N. Trask, M. Maxey, X. Hu, A compatible high-order meshless method for the Stokes equations with applications to suspension flows, Journal of Computational Physics 355 (2018) 310 – 326. doi:https://doi.org/10.1016/j.jcp.2017.10.039.
URL http://www.sciencedirect.com/science/article/pii/S0021999117308069

[19] A. Vázquez-Quesada, P. Español, R. I. Tanner, M. Ellero, Shear thickening of a non-colloidal suspension with a viscoelastic matrix, Journal of Fluid Mechanics 880 (2019) 10701094. doi:10.1017/jfm.2019.753.

[20] X. Bian, M. Ellero, A splitting integration scheme for the SPH simulation of concentrated particle suspensions, Computer Physics Communications 185 (1) (2014) 53 – 62. doi:https://doi.org/10.1016/j.cpc.2013.08.015.
URL http://www.sciencedirect.com/science/article/pii/S0010465513002786

[21] A. Vázquez-Quesada, M. Ellero, Analytical solution for the lubrication force between two spheres in a bi-viscous fluid, Physics of Fluids 28 (7) (2016) 073101. arXiv:https:

//aip.scitation.org/doi/pdf/10.1063/1.4954815, doi:10.1063/1.4954815.
URL https://aip.scitation.org/doi/abs/10.1063/1.4954815

[22] A. Vázquez-Quesada, N. J. Wagner, M. Ellero, Normal lubrication force between spherical particles immersed in a shear-thickening fluid, Physics of Fluids 30 (12) (2018) 123102. arXiv:https://doi.org/10.1063/1.5054067, doi:10.1063/1.5054067.
URL https://doi.org/10.1063/1.5054067

[23] S. S. Prasanna Kumar, A. Vázquez-Quesada, M. Ellero, Numerical investigation of the rheological behavior of a dense particle suspension in a biviscous matrix using a lubrication dynamics method, Journal of Non-Newtonian Fluid Mechanics 281 (2020) 104312. doi:https://doi.org/10.1016/j.jnnfm.2020.104312.
URL http://www.sciencedirect.com/science/article/pii/S037702572030080X

[24] S. Kim, S. Karrila, Microhydrodynamics: Principles and Selected Applications, Butterworth - Heinemann series in chemical engineering, Dover Publications, 2005.

[25] A. J. Banchio, J. F. Brady, Accelerated Stokesian dynamics: Brownian motion, The Journal of Chemical Physics 118 (22) (2003) 10323–10332. arXiv:https://doi.org/10.1063/1.1571819, doi:10.1063/1.1571819.
URL https://doi.org/10.1063/1.1571819

[26] A. K. Townsend, H. J. Wilson, Anomalous effect of turning off long-range mobility interactions in Stokesian dynamics, Physics of Fluids 30 (7) (2018) 077103. arXiv:https://doi.org/10.1063/1.5031860, doi:10.1063/1.5031860.
URL https://doi.org/10.1063/1.5031860

[27] D. I. Dratler, W. R. Schowalter, Dynamic simulation of suspensions of non-Brownian hard spheres, Journal of Fluid Mechanics 325 (1996) 5377. doi:10.1017/S0022112096008038.

[28] A. Sierou, J. F. Brady, Rheology and microstructure in concentrated noncolloidal suspensions, Journal of Rheology 46 (5) (2002) 1031–1056. arXiv:https://doi.org/10.

1122/1.1501925, doi:10.1122/1.1501925.
URL https://doi.org/10.1122/1.1501925

[29] J. F. Brady, G. Bossis, The rheology of concentrated suspensions of spheres in simple shear flow by numerical simulation, Journal of Fluid Mechanics 155 (1985) 105129. doi:10.1017/S0022112085001732.

[30] R. Mari, R. Seto, J. F. Morris, M. M. Denn, Shear thickening, frictionless and frictional rheologies in non-Brownian suspensions, Journal of Rheology 58 (6) (2014) 1693–1724. arXiv:https://doi.org/10.1122/1.4890747, doi:10.1122/1.4890747.
URL https://doi.org/10.1122/1.4890747

[31] C. Ness, J. Sun, Flow regime transitions in dense non-Brownian suspensions: Rheology, microstructural characterization, and constitutive modeling, Phys. Rev. E 91 (2015) 012201. doi:10.1103/PhysRevE.91.012201.
URL https://link.aps.org/doi/10.1103/PhysRevE.91.012201

[32] M. Allen, D. Tildesley, Computer simulation of liquids: Second edition, 2017. doi:10.1093/oso/9780198803195.001.0001.

[33] R. D. Groot, P. B. Warren, Dissipative particle dynamics: Bridging the gap between atomistic and mesoscopic simulation, The Journal of Chemical Physics 107 (11) (1997) 4423–4435. doi:10.1063/1.474784.
URL https://doi.org/10.1063/1.474784

[34] J. H. Irving, J. G. Kirkwood, The statistical mechanical theory of transport processes. IV. The equations of hydrodynamics, The Journal of Chemical Physics 18 (6) (1950) 817–829. arXiv:https://doi.org/10.1063/1.1747782, doi:10.1063/1.1747782.
URL https://doi.org/10.1063/1.1747782

[35] E. Bertevas, X. Fan, R. I. Tanner, Simulation of the rheological properties of suspensions of oblate spheroidal particles in a Newtonian fluid, Rheologica Acta 49 (1) (2009) 53. doi:10.1007/s00397-009-0390-8.
URL https://doi.org/10.1007/s00397-009-0390-8

[36] R. G. Cox, H. Brenner, The slow motion of a sphere through a viscous fluid towards a plane surface-II Small gap widths, including inertial effects, Chemical Engineering Science 22 (12) (1967) 1753 – 1777. doi:https://doi.org/10.1016/0009-2509(67)80208-2.
URL http://www.sciencedirect.com/science/article/pii/0009250967802082

[37] A. J. Goldman, R. G. Cox, H. Brenner, Slow viscous motion of a sphere parallel to a plane wall-I. Motion through a quiescent fluid, Chemical Engineering Science 22 (4) (1967) 637 – 651. doi:https://doi.org/10.1016/0009-2509(67)80047-2.
URL http://www.sciencedirect.com/science/article/pii/0009250967800472